Published in final edited form as:
Neuroreport. 2007 February 12; 18(3): 203–207. doi:10.1097/WNR.0b013e3280115942.

Callosal morphology in Williams syndrome: a new evaluation of shape and thickness

Eileen Luders[a], **Margherita Di Paola**[b], **Francesco Tomaiuolo**[e,f], **Paul M. Thompson**[a], **Arthur W. Toga**[a], **Stefano Vicari**[c], **Michael Petrides**[g], and **Carlo Caltagirone**[b,d]

[a]Laboratory of Neuro Imaging, Department of Neurology,UCLA School of Medicine, Los Angeles, California, USA

[b]IRCCS Fondazione Santa Lucia

[c]IRCCS Ospedale Pediatrico Bambino Gesu, Santa Marinella

[d]Tor Vergata University, Roma

[e]MEYER Ospedale Pediatrico

[f]Dipartimento di Scienze dell'educazione, Università di Firenze, Firenze, Italy

[g]Montreal Neurological Institute, McGill University, Montreal, Quebec, Canada

Abstract

We applied novel mesh-based geometrical modeling methods to calculate and compare the thickness of the corpus callosum at high spatial resolution and to create pro¢les of average callosal shape in a well-matched sample (*n*=24) of individuals with Williams syndrome and controls. In close agreement with previous observations, superimposed surface maps indicate that the corpus callosum in Williams syndrome individuals is shorter and less curved. Moreover, we observed significantly thinner callosal regions in Williams syndrome individuals across the posterior surface, where group effects were less pronounced and spatially restricted in brain-size-adjusted data compared with native data. Circumscribed structural alterations in callosal morphology might be candidate anatomic substrates for the unique cognitive and behavioral profile associated with Williams syndrome.

Keywords

bending; corpus callosum; isthmus; magnetic resonance imaging; morphology; shape; splenium

Introduction

Williams syndrome (WS) is a rare genetically determined disorder with an estimated incidence of one in 20–30 000 births. Affected individuals show a unique cognitive and behavioral profile [1] accompanied by brain abnormalities at the cellular and gross anatomical level involving cerebellar as well as cortical and subcortical structures [2]. Recent studies also suggest abnormal asymmetry patterns and differential hemispheric

Correspondence and requests for reprints to Dr Arthur W. Toga, PhD, Laboratory of Neuro Imaging, Department of Neurology, UCLA School of Medicine 635 Charles Young Drive South, Suite 225, Los Angeles, CA 90095-7334, USA Tel: + 1310 206 2101; fax: + 1 310 206 5518; toga@loni.ucla.edu.

Information on the National Centers for Biomedical Computing can be obtained from http://nihroadmap.nih.gov/bioinformatics.

effects associated with WS [2]. The corpus callosum, the largest interhemispheric commissure known to modulate cerebral specialization and interhemispheric communication, is thus an attractive candidate in exploring the anatomical substrate underlying some of the unique behavioral and cognitive aspects associated with WS. Previous studies indicate a diminished overall area/volume in WS patients, with particularly decreased dimensions in posterior callosal regions [3–5]. Moreover, callosal midline lengths were found to be reduced and callosal bending angles were enlarged [5,6]. That is, the corpus callosum was shorter and less curved in individuals with WS compared with controls. Notwithstanding, contrasting reports exist indicating a lack of callosal differences between WS and control subjects [7].

The present study was designed to shed light on the presence and direction of WS-related disease effects on callosal morphology. Various attempts have been made to subdivide the corpus callosum into anatomically and functionally distinct subareas [8]. Previously, examinations of the corpus callosum in WS were based on predefined callosal regions according to the well-established Witelson segmentation criteria [9], which have recently generated some controversy with respect to the assumed topography of callosal fibers [10]. Moreover, it was demonstrated that misleading outcomes may be obtained when using parcellation methods without taking into account callosal shape [11]. To circumvent the risk of defining callosal sections with controversial fiber distribution, to avoid shape-induced biases, and also to increase the spatial resolution of callosal measurements, we did not rely on any parcellation scheme. Instead, we applied anatomical mesh-based geometrical modeling methods to compute 100 pointwise indicators for callosal thickness across the whole corpus callosum at midline [12,13]. We set out to generate color-coded maps indicating callosal mean thickness (within groups) and significant differences between groups. To visualize size and shape differences in callosal surface anatomy (rather than compare the callosal bending angle [5,6]), we additionally aimed to create and overlay group-specific profiles of average callosal shape. Finally, previous analyses revealed that callosal measurements and related effects of WS are affected by brain size adjustments [5], so we conducted callosal thickness analyses in native space, as well as in scaled space.

Participants and methods

Participants

We analyzed the brain scans of 12 participants with WS (seven men: mean age 20±7.2 years, age range 13–30 years; five women, mean age 16.6±3.01 years, age range 13–20 years) and 12 healthy individuals matched for age and sex (seven men, 20±6.9 years, age range 13–29 years; five women, 16±3.46 years, age range 13–19 years). This same cohort was analyzed and described in Tomaiuolo *et al*. [5]. Handedness was determined by referring to self-reports of hand preference for writing and drawing. Right-handedness was confirmed for 10 out of 12 participants, in each of the WS and control groups. The remaining two participants in each group indicated that they used their left hand for writing and drawing. The neuropsychological profile of WS participants was characterized by a relative preservation of linguistic abilities, whereas visual-spatial processing ability was severely impaired. The diagnosis of WS was made by a pediatric geneticist and subsequently confirmed with molecular analysis. All participants gave informed consent for participation in the study, which was approved by the appropriate institutional ethics committee.

Image acquisition

Magnetization prepared rapid gradient echo T1-weighted images with 1 mm isotropic voxels were obtained with a Siemens 1.5-T Vision Magnetom MR system (Erlangen, Germany)

using the following parameters: TR=11.4 ms; TE=4.4 ms; 15° flip angle. Scans were obtained and preprocessed at the IRCCS Fondazione Santa Lucia (Rome, Italy), and image analysis was performed at the UCLA Laboratory of Neuro Imaging (Los Angeles, California, USA).

Image preprocessing

Radiofrequency bias field corrections were applied to all images, to eliminate intensity drifts due to magnetic field inhomogeneities. To obtain measurements in callosal native space, each image volume was manually positioned along the anterior–posterior commissure line and rotated so that the septum pellucidum and at least a large part of the falx would be visible in the sagittal plane. To adjust callosal measurements for individual and group differences in brain size, a second set of data was created by linearly registering each brain volume to the Montreal Neurological Institute 305-template using a nine-parameter registration algorithm, hereafter referred to as data in scaled space.

Callosal thickness analysis

The corpus callosum was outlined in native space (after anterior–posterior commissure line alignment) and also in scaled space (after applying nine-parameter transformations). One rater (E.L.), who was blind to group status, identified the corpus callosum in midsagittal sections and delineated the upper (top) and lower (bottom) callosal boundaries (Fig. 1a). For inter-rater reliability, two independent investigators contoured the corpus callosum in six different randomly selected brains, achieving intraclass correlation coefficients of r=0.99. Callosal top and bottom sections were redigitized, resulting in 100 equidistant points along the midsagittal callosal curve per section (Fig. 1b). Then a new callosal outline (medial curve) was created by computing the spatial mean curve from surface points representing the top and bottom traces (Fig. 1c), followed by calculating the pointwise distances from the medial curve to the callosal top and bottom curves. The resulting distance values in each participant can be color-coded and superimposed onto each individual's callosal model (Fig. 1d). Subsequently, individual callosal surfaces and pointwise distance values were averaged within groups in order to create (i) group-specific profiles of average callosal shape, as well as (ii) color-coded maps of callosal mean thickness. Finally, we tested for group differences in callosal thickness and generated (iii) color-coded maps illustrating statistically significant regions in which patients with WS differ from healthy individuals (Fig. 1, right panel).

Given that independent sample Student's *t*-tests were made at many callosal surface points and adjacent data points are highly correlated, permutation testing was employed to control for multiple comparisons. For this purpose, callosal sections were randomly assigned to either patient or control groups 100 000 times (although keeping the number of participants in each group the same), and a new statistical test was performed at each callosal surface point for each random assignment. The number of significant results from these randomizations was then compared with the number of significant results in the true assignment to produce a corrected overall significance value for the uncorrected statistical maps. Permutation was conducted both for negative disease effects (controls > WS) and for positive disease effects (WS > controls), as well as for results in native and scaled space.

Results

Callosal shape and mean thickness

We observed profound differences in callosal size and shape between WS patients and healthy individuals (Fig. 2, top panel). That is, although the corpus callosum of WS patients is considerably shorter in general (more noticeable in native space), it is also much less curved (more evident in scaled data).

The regional patterns of callosal thickness are similar in WS and controls, and do not alter noticeably when data are analyzed in scaled versus native space (Fig. 2, bottom panel). Callosal thickness is largest where the callosal body bends near its anterior and posterior ends. The averaged distances from the upper and lower callosal boundaries to midline attain values as high as 6.1 mm, indicating a maximum callosal thickness of 12.2 mm. The corpus callosum was thinnest at its anterior tip, where upper and lower callosal boundaries merge into each other. The callosal main body in the control group appears rather homogeneous (distance values range between 3.0 and 3.5 mm), but callosal distances in the WS group decrease noticeably (distance values are as low as 1.00–2.00 mm) adjacent to the bulbous posterior end (corresponding to the callosal isthmus, according to traditional segmentation schemes).

Group differences in callosal thickness

When callosal data were analyzed in native space (Fig. 3, left panel), we observed significantly thinner callosal regions in WS patients compared with healthy individuals across the whole posterior profile of the corpus callosum (corresponding to the posterior body, isthmus, and splenium). Group differences, however, were less pronounced when callosal thickness was compared in scaled data (Fig. 3, right panel); regions in which the corpus callosum was thinner in WS individuals became restricted to the isthmus and mainly the anterior splenial region. Permutation tests were significant (native space: $P \leq 0.0134$, corrected; scaled space: $P \leq 0.0473$, corrected), indicating that the above-described negative disease effects (controls > WS) do not occur by chance.

Both in the native and scaled space, there was a small area of significantly increased callosal thickness in patients with WS compared with healthy individuals, located near the anterior bend within the callosal anterior third. The final corrected *P* value (revealed by permutation testing) for this positive disease effect (WS > controls), however, did not attain the threshold of significance (native space: $P \leq 0.069$; scaled space: $P \leq 1.000$).

Discussion

In this study, we applied novel computational mesh-based methods to calculate and compare callosal thickness at high spatial resolution and to create profiles of average callosal shape in a well-matched sample of WS individuals and healthy individuals. We revealed shorter and less-curved corpora callosa in WS individuals, as well as significantly thinner callosal regions across the posterior surface of the corpus callosum. In agreement with previous observations on the same sample [5], callosal thickness differences were less pronounced and spatially restricted when data were compared in scaled space versus native space. Notwithstanding, the present study not only confirms previous global and segment-specific effects, but also indicates the exact region of altered callosal morphology with an excellent spatial resolution (Fig. 3).

Our findings corroborate previous reports of reduced posterior callosal regions [3–5], diminished callosal length [6], and enlarged bending angles [5,6] associated with WS. In addition, the observed unique callosal morphology agrees with recent observations of disproportionate reductions in cerebral white matter volume [14,15] and aberrant water content distributions in the corpus callosum [5] in WS individuals. Moreover, our findings indicate that group effects of callosal thickness are located predominantly caudally and may thus accompany other micro-anatomical and macro-anatomical abnormalities associated with WS shown to affect posterior brain regions, such as increased cell size, decreased cell packing density, and abnormal neuronal organization patterns in the primary visual cortex [16,17], as well as unusual gyrification patterns and diminished gray matter in the parietal–occipital cortical region [2,4,14,15,18–22].

The topographic organization of callosal fibers and the positive relationships between total or partial callosal size and small diameter fibers [23] suggest that circumscribed structural alterations in callosal morphology are candidate anatomic substrates for some of the most prominent cognitive and behavioral characteristics of WS individuals, such as profound visuo-spatial deficits [1]. Our observation of diminished callosal thickness in posterior regions may further relate to anomalous brain activations during visual processing and visuo-spatial impairments observed in this population [24,25]. Moreover, aberrations in callosal morphology might be associated with previous observations of abnormal functional and structural asymmetry patterns in WS [2]. Other indirect consequences on WS-specific behavioral anomalies are possible via modulating effects of callosal shape and overall size on the morphology of adjacent structures, which are part of the executive attention network and are also implicated in the processing of emotions and control of social behavior (e.g. the cingulate). The extent to which this morphological profile is related to attentional deficits, hyperactivity, and concentration problems, or to the abnormally excessive social behavior in WS participants [1] remains to be established. Against this background, future studies should also help determine whether the observed increased thickness near the anterior callosal bend in patients with WS is associated with their disturbances in executive functions, or whether this particular disease effect (WS > controls) constitutes a false-positive finding, given that it was not confirmed by permutation testing.

Conclusion

The corpus callosum of WS individuals appears to be shorter, less curved, and significantly thinner in posterior callosal regions compared with controls. These observed structural alterations in callosal morphology might be associated with the unique cognitive and behavioral profile of WS participants.

Acknowledgments

Sponsorship: This publication was made possible by Grant numbers P41 RR013642 and M01 RR000865 from the National Center for Research Resources (NCRR), a component of the National Institutes of Health (NIH). Algorithm development was partly supported by grants from the National Institute for Biomedical Imaging and Bioengineering, the National Center for Research Resources, and the National Institute on Aging (EB01651, RR019771, AG016570 to P.M.T.). Additional support was provided by the National Institutes of Health through the NIH Roadmap for Medical Research, Grant U54 RR021813 entitled Center for Computational Biology (CCB).

References

1. Mervis CB, Klein-Tasman BP. Williams syndrome: cognition, personality, and adaptive behavior. Ment Retard Dev Disabil Res Rev. 2000; 6:148–158. [PubMed: 10899809]
2. Gaser C, Luders E, Thompson PM, Lee AD, Dutton RA, Geaga JA, et al. Increased local gyrification mapped in Williams syndrome. Neuroimage. 2006; 33:46–54. [PubMed: 16901723]
3. Schmitt JE, Eliez S, Warsofsky IS, Bellugi U, Reiss AL. Corpus callosum morphology of Williams syndrome: relation to genetics and behavior. Dev Med Child Neurol. 2001; 43:155–159. [PubMed: 11263684]
4. Galaburda AM, Bellugi UV. Multi-level analysis of cortical neuroanatomy in Williams syndrome. J Cogn Neurosci. 2000; 12(Suppl 1):74–88. [PubMed: 10953235]
5. Tomaiuolo F, Di Paola M, Caravale B, Vicari S, Petrides M, Caltagirone C. Morphology and morphometry of the corpus callosum in Williams syndrome: a T1-weighted MRI study. Neuroreport. 2002; 13:2281–2284. [PubMed: 12488811]
6. Schmitt JE, Eliez S, Bellugi U, Reiss AL. Analysis of cerebral shape in Williams syndrome. Arch Neurol. 2001; 58:283–287. [PubMed: 11176967]
7. Wang PP, Doherty S, Hesselink JR, Bellugi U. Callosal morphology concurs with neurobehavioral and neuropathological findings in two neurodevelopmental disorders. Arch Neurol. 1992; 49:407–411. [PubMed: 1532713]

8. Peters M, Oeltze S, Seminowicz D, Steinmetz H, Koeneke S, Jancke L. Division of the corpus callosum into subregions. Brain Cogn. 2002; 50:62–72. [PubMed: 12372352]
9. Witelson SF. Hand and sex differences in the isthmus and genu of the human corpus callosum. A postmortem morphological study. Brain. 1989; 112(Pt 3):799–835. [PubMed: 2731030]
10. Hofer S, Frahm J. Topography of the human corpus callosum revisited: comprehensive fiber tractography using diffusion tensor magnetic resonance imaging. Neuroimage. 2006; 32:989–994. [PubMed: 16854598]
11. Tomaiuolo F, Scapin M, Di Paola M, Le Nezet P, Fadda L, Caltagirone C, et al. Gross anatomy of the corpus callosum in Alzheimer's disease: regions of degeneration and their neuropsychological correlates. Dement Geriatr Cogn Disord. 2007; 23:96–103. [PubMed: 17127820]
12. Luders E, Narr KL, Zaidel E, Thompson PM, Jancke L, Toga AW. Parasagittal asymmetries of the corpus callosum. Cereb Cortex. 2006; 16:346–354. [PubMed: 15901651]
13. Luders E, Narr KL, Zaidel E, Thompson PM, Toga AW. Gender effects on callosal thickness in scaled and unscaled space. Neuroreport. 2006; 17:1103–1106. [PubMed: 16837835]
14. Reiss AL, Eliez S, Schmitt JE, Straus E, Lai Z, Jones W, et al. IV. Neuroanatomy of Williams syndrome: a high-resolution MRI study. J Cogn Neurosci. 2000; 12(Suppl 1):65–73. [PubMed: 10953234]
15. Thompson PM, Lee AD, Dutton RA, Geaga JA, Hayashi KM, Eckert MA, et al. Abnormal cortical complexity and thickness profiles mapped in Williams syndrome. J Neurosci. 2005; 25:4146–4158. [PubMed: 15843618]
16. Galaburda AM, Holinger DP, Bellugi U, Sherman GF. Williams syndrome: neuronal size and neuronal-packing density in primary visual cortex. Arch Neurol. 2002; 59:1461–1467. [PubMed: 12223034]
17. Galaburda AM, Wang PP, Bellugi U, Rossen M. Cytoarchitectonic anomalies in a genetically based disorder: Williams syndrome. Neuroreport. 1994; 5:753–757. [PubMed: 8018845]
18. Reiss AL, Eckert MA, Rose FE, Karchemskiy A, Kesler S, Chang M, et al. An experiment of nature: brain anatomy parallels cognition and behavior in Williams syndrome. J Neurosci. 2004; 24:5009–5015. [PubMed: 15163693]
19. Meyer-Lindenberg A, Kohn P, Mervis CB, Kippenhan JS, Olsen RK, Morris CA, et al. Neural basis of genetically determined visuo-spatial construction deficit in Williams syndrome. Neuron. 2004; 43:623–631. [PubMed: 15339645]
20. Van E, Dierker D, Snyder AZ, Raichle ME, Reiss AL, Korenberg J. Symmetry of cortical folding abnormalities in Williams syndrome revealed by surface-based analyses. J Neurosci. 2006; 26:5470–5483. [PubMed: 16707799]
21. Kippenhan JS, Olsen RK, Mervis CB, Morris CA, Kohn P, Meyer-Lindenberg A, et al. Genetic contributions to human gyrification: sulcal morphometry in Williams syndrome. J Neurosci. 2005; 25:7840–7846. [PubMed: 16120786]
22. Schmitt JE, Watts K, Eliez S, Bellugi U, Galaburda AM, Reiss AL. Increased gyrification in Williams syndrome: evidence using 3D MRI methods. Dev Med Child Neurol. 2002; 44:292–295. [PubMed: 12033713]
23. Aboitiz F, Scheibel AB, Fisher RS, Zaidel E. Fiber composition of the human corpus callosum. Brain Res. 1992; 598:143–153. [PubMed: 1486477]
24. Grice SJ, Haan MD, Halit H, Johnson MH, Csibra G, Grant J, et al. ERP abnormalities of illusory contour perception in Williams syndrome. Neuroreport. 2003; 14:1773–1777. [PubMed: 14534418]
25. Mobbs D, Garrett AS, Menon V, Rose FE, Bellugi U, Reiss AL. Anomalous brain activation during face and gaze processing in Williams syndrome. Neurology. 2004; 62:2070–2076. [PubMed: 15184616]

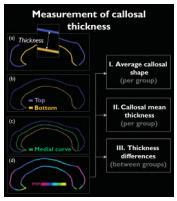

Fig. 1.

Illustration of callosal thickness measurements. Left panels (a–d): after delineating and redigitizing upper and lower callosal boundaries (top and bottom), we computed the spatial mean (medial curve) between points representing the top and bottom. The pointwise distances between medial curve (green) and callosal top (blue) and bottom (yellow) segments were calculated and superimposed as color-coded values onto each participant's callosal surface model. Right panels [I–III]: individual callosal surfaces and pointwise distance values were averaged within groups to create profiles of average callosal shape and maps of callosal mean thickness within groups, as well as significance maps representing regions in which groups differ with respect to callosal thickness.

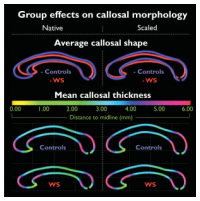

Fig. 2.

Group effects on callosal morphology. Illustrated are callosal shape profiles of Williams syndrome (WS) patients and controls. Posterior (caudal) callosal regions point to the right and anterior (rostral) regions to the left (top panel). Group-specific callosal thickness profiles are displayed as color-coded maps, illustrating the averaged distances (mm) between the upper/lower boundaries and callosal medial line (bottom panel). Smaller distances correspond to a decreased callosal thickness, and larger distances correspond to an increased callosal thickness. Results shown in the left panel are based on analyses in native space; findings on the right refer to scaled space.

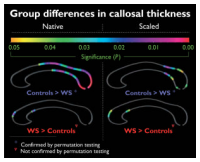

Fig. 3.

Group differences in callosal thickness. Illustrated are regions of significant differences in callosal thickness between Williams syndrome (WS) patients and controls. The color bar encodes the *P* value associated with the *t*-test performed at each distance value from upper and lower callosal boundaries. Permutation tests were significant for the comparison of controls > WS (both in native and scaled space), but not significant for the findings of WS > controls. Results shownin the left panelare based on analyses in native space; findings on the right refer to scaled space.